Calcitonin suppresses intervertebral disk degeneration and preserves lumbar vertebral bone mineral density and bone strength in ovariectomized rats

F.-m. Tian[1] · K. Yang[2] · W.-y. Wang[3] · Y. Luo[4] · S.-y. Li[2] ·
H.-p. Song[2] · Y.-z. Zhang[4] · Y. Shen[4] · L. Zhang[2]

Abstract

Summary We investigated the effect of calcitonin (CT) on lumbar intervertebral disk degeneration (LIDD) in rats with ovariectomy-induced osteopenia. CT protected ovariectomized rats from LIDD by, at least in part, modifying extracellular matrix metabolism of the disks and preserving the microarchitecture and biomechanical properties of adjacent vertebrae.

Introduction The present study aimed to investigate the effect of CT on lumbar vertebral bone mineral density and intervertebral disk degeneration in ovariectomized (OVX) rats.

Methods We first subjected 50 3-month-old female rats to either OVX ($n=30$) or sham ($n=20$). Twelve weeks later, ten OVX and ten sham rats were necropsied. The remaining OVX rats began to receive either saline vehicle (OVX+V, $n=10$), or salmon CT (OVX+CT, 16 IU/kg/2 days, $n=10$). After 12 weeks of treatment, necropsy was conducted and bone mineral density was determined in L3–4 and L5–6 vertebrae. The microstructure and biomechanical properties of L3 vertebrae were detected by micro-computed tomography and compression test, respectively. L5–6 was also used to measure intervertebral disk height and observe intervertebral disk histological changes by Van Gieson staining and histological scores, as well as immunohistochemistry (IHC) analysis of matrix metalloprotease (MMP)-1, MMP-13, and collagen II expression.

Results At 12 weeks post-OVX, OVX rats had lower BV/TV and Tb.N and higher intervertebral disk histological score than sham rats. After 24 weeks, OVX+CT rats had higher BMD, BV/TV, Tb.N, and bone biomechanical strength values than OVX+V rats. Histological analysis showed OVX+CT rats had significantly lower disk degeneration scores than OVX+V rats. IHC analysis revealed CT treatment decreased expression of MMP-1 and MMP-13 and increased expression of collagen II compared with OVX+V rats.

Conclusions Our data demonstrate that CT-treated OVX rats display less intervertebral disk degeneration and favorable changes in intervertebral disk metabolism, associated with higher trabecular bone mass, better trabecular microarchitecture, and better biomechanical strength when compared to vehicle-treated OVX rats.

Keywords Biomechanics · Intervertebral disk degeneration · Micro-computed tomography · Osteopenia · Salmon calcitonin

Fa-ming Tian and Kai Yang contributed equally to this work.

✉ L. Zhang
zhliu130@sohu.com

1 Medical Research Center, Affiliated Hospital of Hebei United University, Tangshan, People's Republic of China

2 Department of Orthopedic Surgery, Affiliated Hospital of Hebei United University, No. 73 Jianshe South Rd, Tangshan 063000, Hebei, People's Republic of China

3 Department of Pathology of Basic Medical Sciences School, Hebei United University, Tangshan, People's Republic of China

4 Department of Orthopedic Surgery, The Third Hospital of Hebei Medical University, Shijiazhuang, People's Republic of China

Introduction

Intervertebral disk degeneration is a common musculoskeletal condition. Disk degeneration can progress to disk herniation and spinal canal stenosis and in conjunction with facet joint arthrosis and degenerative spondylolisthesis. Over 90 % of surgical spine operations are performed because of consequences of disk degeneration [1]. The intervertebral disks

are cartilaginous, articulating structures between the vertebral bodies, which allow movement (flexion, extension, and rotation) in the otherwise rigid anterior portion of the vertebral column, and are continually changing as a result of development, aging, and degeneration [2]. Although intervertebral disk degeneration has a multifactorial etiology, involving age, mechanical, genetic, systemic, and toxic factors [3], increasing evidence suggests a relationship between changes in vertebra body and intervertebral disk degeneration.

A correlation study of bone mineral density (BMD) and lumbar disk degeneration in premenopausal and postmenopausal women demonstrated that BMD not only of the lumbar vertebrae but also of the calcaneus and radius is positively associated with lumbar disk degeneration [4]. However, Fabreguet et al. [5] have shown that in osteoporotic men, the prevalence of lumbar spine degeneration is high. Relative estrogen deficiency may contribute to accelerated disk degeneration in postmenopausal females [6]. In addition, our previous studies have revealed a strong association between osteopenia and disk degeneration in OVX rats, and intervention by alendronate, a widely accepted antiresorptive agent, could not only prevent osteopenia but also inhibit intervertebral disk degeneration [7, 8].

Calcitonin (CT) is a 32-amino acid peptide hormone, produced by the parafollicular cells in the thyroid gland, which possesses antiresorptive effects by binding to its receptor on osteoclasts [9]. As another bone resorption inhibitor, CT may also be a potential choice for treatment of intervertebral disk degeneration induced by estrogen deficiency. A previous experimental study revealed that CT reduced biochemical markers of cartilage degradation [10]. Pretreatment with CT exerts an inhibitory action on matrix metalloprotease (MMP)-13 expression in articular chondrocytes, under the influence of IL-1, and regulates expression of collagen II, MMP-3, and ADAMTS-4, contributing to the histological integrity of cartilage [11]. Regarding the cartilage-protective effects of CT, degeneration of the intervertebral disk might be directly inhibited by CT intervention.

Based on current literature, the present study was designed to investigate the effects of CT on the vertebrae by detecting the bone mass, microstructure, and biomechanical properties of the vertebrae using BMD, micro-CT, and compression testing and on intervertebral disk degeneration by histology, disk height measurement, and immunohistochemistry (IHC) analysis in OVX rats.

Materials and methods

Experimental design

Thirty 3-month-old female Sprague–Dawley (SD) rats (Peking University Animal Center, Beijing, China) were used in this study. We first subjected 30 female rats to either dual ovariectomy ($n=30$) or sham operation ($n=20$). Twelve weeks later, ten rats from each group were sacrificed for the bone histomorphometrical assessment and histological analysis. The remaining sham rats received saline vehicle treatment, and the remaining OVX rats received either (1) saline vehicle treatment (OVX+V, $n=10$) or (2) subcutaneous injection of salmon CT (Novartis AG, Switzerland) at a dose of 16 IU/kg/2 days (OVX+CT, $n=10$) [12]. After 12 weeks of treatment, all animals were sacrificed.

Confirmation of bone loss and disk degeneration in rats at week 12

The posterior elements and transverse processes of the L2 vertebrae were removed, and the L2 vertebral body was fixed in 70 % ethanol for 3 days. The L2 vertebral body was then cut in half in the sagittal plane with a low-speed metallurgical saw (SYJ-150, Kejing, China), and both halves were dehydrated in ascending grades of ethanol, defatted in dimethyl benzene, and embedded in methyl-methacrylate without decalcification. Undecalcified 5-μm-thick sections were prepared in the parasagittal plane using a Jung-K microtome (Reichert-Jung, Heidelberg, Germany). The sections were stained with Giemsa; the following parameters were examined using a semiautomatic digitizing system (Leica QWin, Leica, Germany) for bone histomorphometrical assessment, with final magnification of ×200: percent bone volume (BV/TV), trabecular number (Tb.N), trabecular thickness (Tb.Th), and trabecular separation (Tb.Sp), The areas measured were defined as the trabecular bone of the vertebra excluding the region 1 mm from the proximal and distal growth plate.

The L4–5 segments of the lumbar spine (including the intervertebral disk) were fixed in neutral-buffered 10 % formalin for 5 days and decalcified in 10 % disodium–ethylenediaminetetraacetic acid (EDTA-2Na) for 3 months and then split down the mid-sagittal plane with a scalpel and embedded in paraffin. Samples were then cut into 5-μm-thick sections in the parasagittal plane, placed on microscope slides, and stained with Van Gieson (VG) for light microscopic examination.

Degenerative changes in the intervertebral disks were observed and the degrees of change in the stained sections were scored independently by three individuals blinded to the experimental protocol, using the disk degeneration assessment scoring system (Table 1) described by Wang et al. [7].

Assessments at week 24

BMD assessment

At week 24, L34 and L5-6 segments from all animals were dissected, freed from adjacent soft tissue, and preserved in

Table 1 Lumbar intervertebral disk degeneration assessment scoring system

Score	Nucleus pulposus	Annulus fibrosus	Osteophyte
0	Bulging gel with abundant notochordal cells	Compact fibrous lamellas	Absence
1	Notochordal cells loss; chondrocyte-like cell emergence	Proliferation of fibrocartilaginous tissue and loss of nuclear–annular border	Appearance
2	Focal mucoid degeneration; clefts	Fissures in annulus fibrosis	Overgrowth
3	Diffuse mucoid degeneration and clefts throughout the nucleus		

The maximum possible histological score for any section is 7 points. It is the sum of 3 possible points for the nucleus pulposus, 2 possible points for the annulus fibrosus, and 2 possible points for osteophyte

70 % ethanol for 1 day. BMD of L3-4 and L5-6 was performed on the anteroposterior plane, by dual-energy X-ray absorptiometry using a densitometer (QDR Discovery, Hologic, Bedford, MA, USA) operating at high-resolution mode and specialized software for small animals supplied by the equipment manufacturer.

Micro-CT measurements

3D analysis was performed on the trabeculae of the cancellous tissue of the L3 vertebrae, using a SkyScan 1076 micro-CT (SkyScan, Aartselaar, Belgium). The micro-CT equipment comprised a microfocus X-ray tube with a focal spot of 9 μm to produce a fan beam detected by a charge-couple device array and a turntable that could be shifted automatically in the axial direction. The energy and intensity were equal to 40 kVp and 250 μA, respectively. On the original 3D images, morphometric indices were directly determined from the volume of interest (VOI), which was restricted to an inner cylinder with 1.5-mm diameter and the trabecular bone of entire vertebrae excluding the region 1 mm from the junction of the growth cartilage with the metaphysis of the proximal and distal growth plate. The following 3D morphometric parameters were calculated to describe the bone mass and microstructure: BV/TV, Tb.N, Tb.Th, Tb.Sp, and structural model index (SMI).

Biomechanical testing

Using a table mount mechanical strength analyzer (AG-IS 10kN, SHIMADZU, Japan), the mechanical strength of the lumbar vertebrae (L3) was measured by compression test [13]. In this test, the posterior elements and transverse processes were removed, the planoparallel surfaces were obtained by removing the cranial and caudal ends of the vertebral specimen, and then, the vertebral body test specimen with planoparallel ends was obtained by using a file to smooth the cranial and caudal sides of each sample. All compression tests were performed in the displacement-control mode at a crosshead speed of 0.5 mm/min to eliminate any strain rate effects. Maximum load was read automatically from the load–deformation curve, which was recorded by the Trapezium 2

(version 2.10) and exported into the Microsoft Excel, yield stress and maximum stress were obtained as the division of yield load and maximum load by the cross-sectional area of the vertebrae, respectively, vertebral cross-sectional area was calculated by the ratio of vertebral volume/vertebral height, and vertebral volume was obtained by the formula as follows: [(vertebra wet weight−vertebra weight in water)/water density×gravity acceleration], and the height of the vertebral body was measured with a vernier caliper. Elastic modulus was calculated by the formula KL/A based on the data of stiffness (K, the slope of load–deformation curve in elastic region), length (L, the height of vertebral body test specimen), and area (A) of the vertebrae.

Disk height measurement and histological evaluation

After the BMD test, the L5-6 segments of the lumbar spine (including the intervertebral disk) were fixed in neutral-buffered 10 % formalin for 5 days, decalcified in 10 % EDTA-2Na for 3 months, split down at the mid-sagittal plane with a scalpel, and embedded in paraffin. Samples were then cut into 5-μm-thick parasagittal plane sections, placed on microscope slides, and stained with VG for light microscopic examination.

Disk height measurements were taken from the caudal aspect of the growth plate of L5 to the cranial aspect of the growth plate of L6 on histological samples from the L5-6 segments. For each image that projected from a microscope through a camera onto a computer screen, the height was determined under×12.5 magnification using a semiautomatic digitizing system (Cell Sens Version. 1.8, Olympus Soft Imaging solutions GmbH, Germany) with 300 dpi of resolution, with an average of three measurements made in three areas of the disk space for one section from each rat: one at the anterior, one at the central, and one at the posterior side (Fig. 2) [14]. The operator was blinded to the identification of the slide as blind-coded slides were presented to the operator in random order. The coefficient of variation of three measurements of the same IDH site taken by the same investigator over a 1-week period was 0.007.

Degenerative changes in the intervertebral disks were observed from one section per rat, and the degrees of change in

the stained sections were scored independently by three individuals blinded to the identification of the slide as blind-coded slides were presented in random order, using the disk degeneration assessment scoring system (Table 1) described by Wang et al. [7].

Immunohistochemistry analysis

Tissue sections from L5-6 segments were deparaffinized in xylene and rehydrated in a reverse-graded series of ethanol. After antigen retrieval, quenching of endogenous peroxidase and blocking of non-specific binding, sections were incubated overnight at 4 °C with either antirat MMP-1, MMP-13, or collagen II (1:100; all from Bioss, Inc., Beijing, China). The remaining procedures were performed according to the SA1066 SABC-FITC kit (Boster Corporation, Wuhan, China), and the color (brown) was developed by incubation in DAB (ZSGB-BIO Corporation, Beijing, China). Sections were counterstained with hematoxylin. The samples appearing yellow or brownish yellow were considered as positive staining. All sections were semiquantitatively analyzed by Image Pro Plus (IPP) version 6.0 software, and the integrated optical density (IOD) was measured from staining of six fields for each section using one section per rat, on the images at ×400 magnification [8, 15]. The average IOD from three observers was the final observation result and used for statistical analysis.

Statistical analysis

All data were analyzed using SPSS 15.0 software, and results are expressed as mean±SD. The statistical significance between groups was estimated using one-way analysis of variance (ANOVA) and Fisher's protected least significant difference test. The results of histological scores were analyzed using a non-parametric test of Kruskal–Wallis, followed by Fisher's protected least significant difference post hoc test. Spearman correlation was done to analyze the relationship between L5-6 BMD and histological scores. P values less than 0.05 were considered statistically significant.

Results

Histomorphometrical findings and histological changes in rats at week 12

Histomorphometrical assessment showed that BV/TV, Tb.Th, and Tb.N in OVX rats were significantly lower than those in sham rats, and significantly higher Tb.Sp was observed in OVX rats in comparison with sham rats (Table 2).

As shown in Fig. 1, in comparison with sham rats, OVX rats exhibited mild degeneration as the cartilage layers in end

Table 2 The results of bone histomorphometrical analysis and histological score at week 12

	Sham	OVX
Histomorphometrical test		
BV/TV (%)	38.5±2.18	29.03±2.95*
Tb.Th (μm)	110.6±9.5	95.5±13.7*
Tb.N (/mm)	3.50±0.28	2.25±0.14*
Tb.Sp (μm)	176.8±19.1	317.3±27.1*
Histological score	1.18±0.47	3.02±1.24*

Data are expressed as mean±SD

BV/TV percent bone volume, *Tb.Th* trabecular thickness, *Tb.N* trabecular number, *Tb.Sp* trabecular separation

plates were decreased and were partially replaced by calcified tissues. Loss of cellularity of notochordal cells was observed in the nucleus pulposus, mucoid degeneration was also observed in the posterior part of the nucleus pulposus, and disruption of the nuclear–annular border was observed at the annulus fibrosus (Fig. 1). Histological score of the disks in the OVX rats was significantly higher than that in the sham rats ($P<0.05$) (Table 2).

Bone mineral density of L3-4 and L5-6

At week 24, BMD of L3-4 and L5-6 in the OVX+V was significantly lower than that in the Sham rats, and BMD of L5-6 in OVX+CT rats was significantly lower than that in the Sham rats. OVX+CT rats showed significantly higher BMD of both L3-4 and L5-6 than OVX+V rats (Table 3).

Micro-CT analysis of L3 vertebrae

Quantification of 3D trabecular structures revealed that in the OVX+V rats, BV/TV and Tb.N were significantly decreased ($P<0.05$) and Tb.Sp was significantly higher ($P<0.05$), compared with the sham rats and OVX+CT rats. OVX+CT rats had BV/TV, Tb.N, Tb.Th, and Tb.Sp values comparable to those of sham rats (Table 3).

Biomechanical properties of L3

As shown in Table 3, the maximum load, yield stress, maximum stress, and elastic modulus in the OVX+V group were significantly lower than those in the Sham group ($P<0.05$). Furthermore, OVX+CT rats showed markedly higher values compared with the OVX+V group ($P<0.05$), while only the elastic modulus in OVX+CT rats was lower than that in sham rats ($P<0.05$) (Table 3).
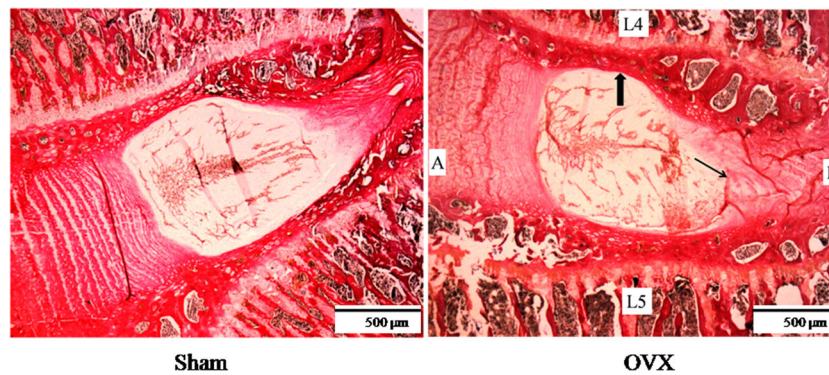
Sham | **OVX**

Fig. 1 Histological assay of the L4-5 segments of the lumbar spine by Van Gieson staining from sham and OVX rats at week 12. In OVX rats, mineralized tissue was more abundant in the deep zone of middle cartilage end plate (*thick arrow*); mild mucoid degeneration occurred in the posterior part of the nucleus pulposus. *A* anterior side, *P* posterior side.

The score of the sham section was 1, as loss of the nuclear–annular border in the posterior part of the nucleus pulposus was observed (1 point). The score of the OVX section was 3, as focal mucoid degeneration (2 points) and loss of the nuclear–annular border (1 point) were observed

Disk height and histological findings

Disk height in the OVX+V group was significantly lower than that in the sham and OVX+CT rats ($P<0.05$), while the value in OVX+CT rats was significantly lower than that of sham rats (Table 3). The sham group appeared to exhibit mild degeneration as the cartilage end plates were partially calcified and a few doublets of chondrocyte-like cells were observed within the

nucleus pulposus at the rear side. In addition to diminished disk height, the OVX+V group experienced degeneration of the end plate, annulus fibrosus, and nucleus pulposus. Mineralized tissue became more obvious in the deep zone of the middle cartilage end plate. The nucleus pulposus exhibited significant loss of cellularity of notochordal cells, which were replaced by chondrocyte-like cells. Mucoid degeneration was also observed to erode the nucleus pulposus, with apparent cleft formation.

Table 3 The results of BMD, biomechanical test, micro-CT, disk height, histological score, and IOD of MMP-1, MMP-13, and collagen II

	Sham	OVX+V	OVX+CT
BMD (g/cm^2)			
L3-4	0.270±0.015	0.232±0.008*	0.257±0.013#
L5-6	0.286±0.011	0.238±0.006*	0.270±0.016*#
Biomechanical test			
Maximum load (N)	188.2±43.6	82.9±31.7*	141.2±47.4#
Yield stress (MPa)	16.5±4.8	6.6±3.0*	11.3±4.2#
Maximum stress (MPa)	19.7±4.5	10.4±1.9*	15.1±2.3#
Elastic modulus (MPa)	706.5±48.9	228.0±47.3*	469.7±75.0*#
Micro-CT			
BV/TV (%)	23.7±4.8	16.0±2.0*	21.2±0.5#
Tb.Th (μm)	101.1±3.2	102.3±3.8	99.3±0.5
Tb.N (/mm)	2.3±0.4	1.6±0.2*	2.1±0.1#
Tb.Sp (μm)	254.6±23.5	367.1±15.0*	266.2±4.6#
SMI	1.31±0.36	1.51±0.11	1.57±0.12
Disk height (mm)	1.29±0.04	1.13±0.05*	1.23±0.04*#
Histological score	2.33±0.47	4.17±0.62*	3.05±0.57*#
IOD			
MMP-1	554±51	865±71*	681±89*#
MMP-13	390±81	783±111*	450±80#
Collagen II	6936±1060	3235±896*	5543±856#

Data are expressed as mean±SD

BV/TV percent bone volume, *Tb.Th* trabecular thickness, *Tb.N* trabecular number, *Tb.Sp* trabecular separation, *SMI* structural model index

*$P<0.05$ vs. the sham group; #$P<0.05$ vs. the OVX+V group

Loss of collagen, proliferation of fibrocartilaginous tissue, and disruption of the nuclear–annular border were observed at the annulus fibrosus. Maintenance of disk integrity was confirmed by 12 weeks of CT treatment, after which the disk appeared less degenerate compared with the OVX+V animals (Fig. 2, Table 3).

At week 24, histological score of the disks in the OVX+V group was significantly higher than that in the sham and OVX+CT groups ($P<0.05$) (Table 3); the maximum score observed in sham, OVX+V and OVX+CT groups is 3, 5, and 4, respectively. The histological score was negatively related to L5-6 BMD. ($r=0.599$, $P=0.018$).

Immunohistochemical staining

As shown in Fig. 3, sham collagen II expression was extensive at the annulus fibrosus, with weak expression of MMP-1 and MMP-13 in the sham rats. OVX+V rats exhibited increased MMP-1 and MMP-13 and weaker collagen II expression. OVX+CT rats exhibited weaker MMP-1 and MMP-13 and stronger collagen II expression, compared with OVX+V rats.

Quantitative analysis indicated higher IOD values for MMP-1 and MMP-13 and a lower IOD value for collagen II in the OVX+V group compared with the sham and OVX+CT groups ($P<0.05$). A lower IOD value for MMP-1 was observed in the OVX+CT group compared with the sham group.

Discussion

Our present findings demonstrate that CT can not only preserve vertebra BMD, biomechanical properties, and trabecular bone microstructure with the exception of SMI but also normalize ECM metabolism of intervertebral disks, through counteracting the enhanced MMP-1 and MMP-13 and diminished collagen II expression in ovariectomized rats.

The relationship between osteopenia and intervertebral disk degeneration remains controversial. Relative estrogen deficiency may contribute to accelerated disk degeneration in postmenopausal females [6]. In a prospective radiographic study of subjects 55 years and older, de Schepper et al. found that disk degeneration was more prevalent in women than in men [16]. Furthermore, elderly females are more likely to have more severe lumbar disk degeneration than elderly males [17, 18]. A positive relationship between radiographic lumbar intervertebral disk height and hormone replacement treatment in postmenopausal women has been reported. In this report, untreated menopausal women were found to have the lowest total lumbar disk height, significantly lower than both premenopausal women and hormone-treated postmenopausal women [19]. The present study shows deterioration of lumbar vertebral body bone microstructure in rats at 12 and 24 weeks after OVX. Furthermore, biomechanical testing showed weaker vertebral body trabecular bone at 24 weeks post-OVX, which was similar to our previous study [7, 8]. Based on the recognition of wide variation in the degenerative changes in intervertebral disk, the use of a grading system pioneered by Wang et al. provides a semiquantitative assessment of the severity of disk degradation in the end plate, nucleus pulposus, and annulus fibrosus [7]. According to the double-blind evaluated scores, intervertebral disk degeneration developed by 12 weeks after OVX and persisted at 24 weeks after ovariectomy. Moreover, calcitonin prevented progressive deterioration of disk integrity. However, in spite
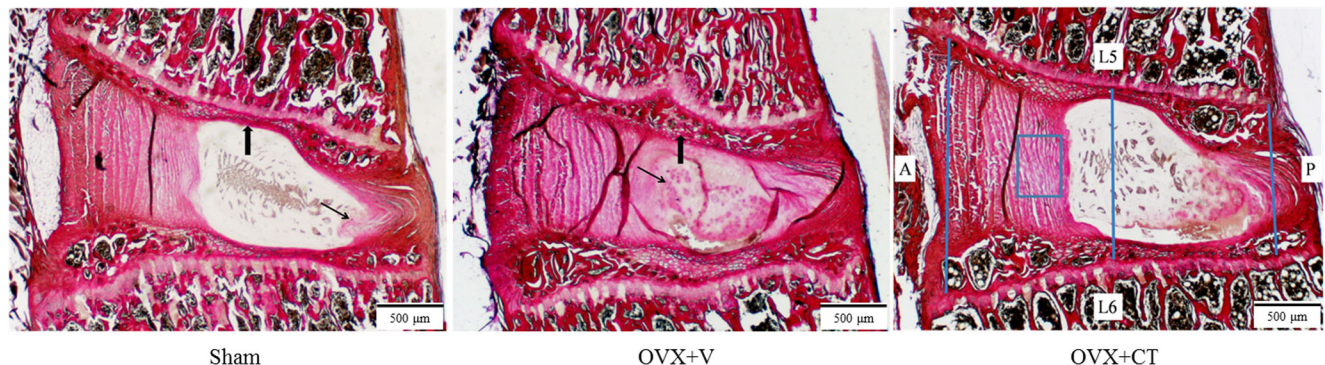

Sham OVX+V OVX+CT

Fig. 2 Histological assay of the L5-6 segments of the lumbar spine by Van Gieson staining. As the *black arrows* indicate, the sham group appear to have mild degeneration as the cartilage end plates partially calcified (*thick arrow*); abundant notochordal cells were observed, while a few doublets of chondrocyte-like cells appeared within the nucleus pulposus at the posterior side (*thin arrow*); in OVX+V group, mineralized tissue was more abundant in the deep zone of middle cartilage end plate (*thick arrow*); the nucleus pulposus appeared to have significant loss of cellularity in notochordal cells and mucoid degeneration (*thin arrow*). The *blue lines* mark the three exact locations where disc height was measured. The *blue rectangle frame* indicates the origin of the tissue shown in Fig. 3. *A* anterior side, *P* posterior side. The score of the sham section was 2, as chondrocyte-like cells appeared (1 point) and loss of the nuclear–annular border in the posterior part of the nucleus pulposus (1 point) was observed. The score of the OVX+V section was 4, as mucoid degeneration (3 points) and loss of the nuclear–annular border (1 point) were observed. The score of the OVX+CT section was 3, as focal mucoid degeneration (2 points) and loss of nuclear–annular border (1 point) were observed
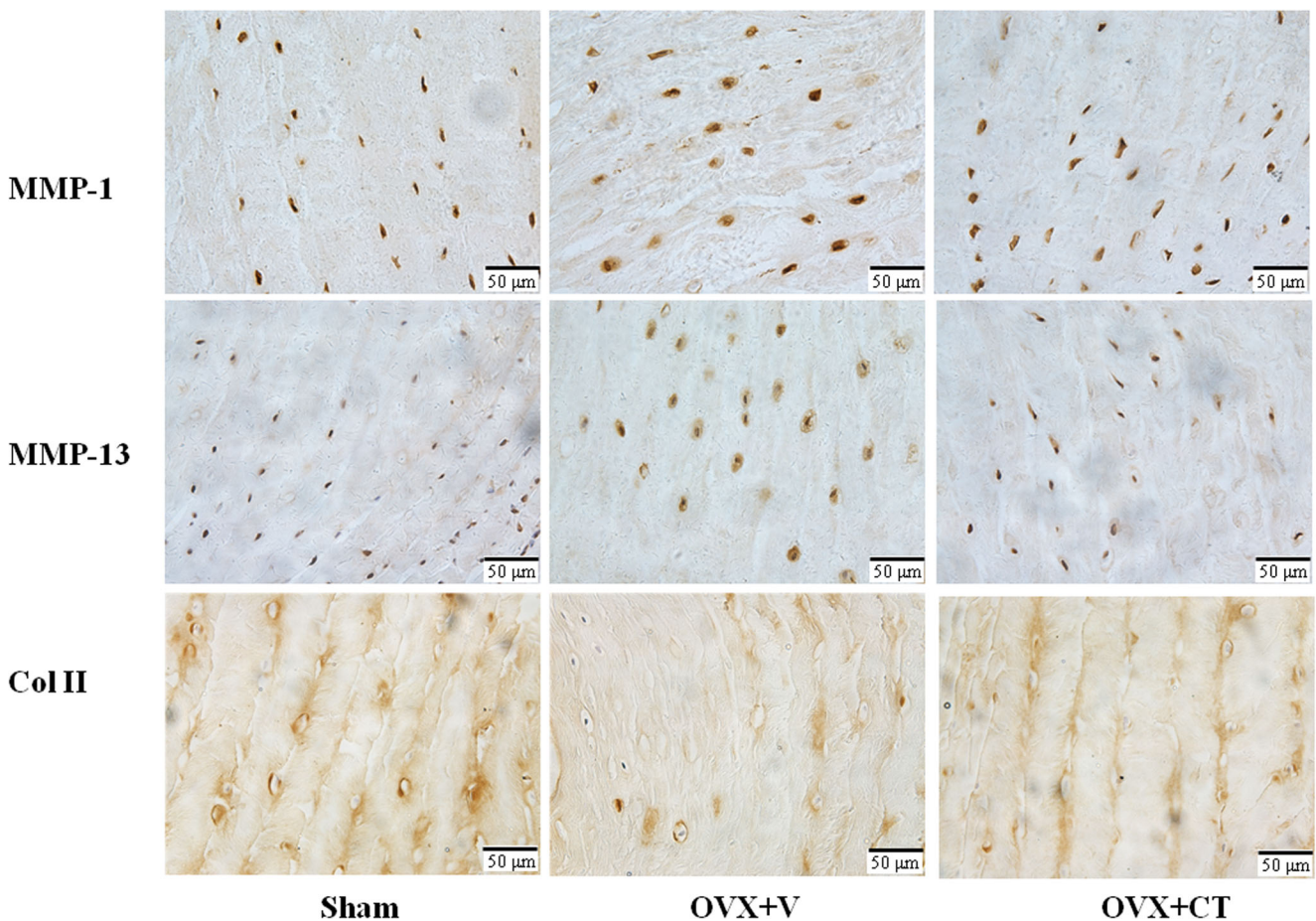
Fig. 3 Immunohistochemistry assay for MMP-1, MMP-13, and collagen II in the annulus fibrosis (×400). Collagen II-positive staining in the annulus fibrosis was much weaker in the OVX+V group than that in the sham and OVX+CT and groups. MMP-1- and MMP-13-positive staining in the annulus fibrosis was stronger in the OVX+V group than in the sham and OVX+CT groups

of the higher values of BV/TV and Tb.N and lower Tb.Sp in OVX+CT rats in comparison with OVX+V rats, the SMI showed no significant difference between the two groups; it is really an unexpected result and difficult to explain.

However, the relationship between osteopenia and disk degeneration is still in debate. Increasing evidence supports that BMD is positively related to disk degeneration, with a higher BMD of the vertebral body being associated with more severe adjacent disk degeneration [20]. Accordingly, lower lumbar spine BMD is associated with less severe disk degeneration [17]. Mattei reviewed the literature regarding the relationship between osteopenia and intervertebral disk degeneration and proposed that osteopenia delays intervertebral disk degeneration, by increasing intradiscal diffusive transport of nutrients through both mechanical and vascular pathophysiological pathways [21]. The contradiction of these results, with regard to the relationship between osteopenia and intervertebral disk degeneration, is difficult to explain. However, it must be kept in mind that although BMD is the gold standard for diagnosis of osteoporosis, some other additional changes contribute to the pathogenesis of osteoporosis, especially when induced by

ovariectomy. First, estrogen deficiency is a main cause of bone loss in postmenopausal women. In addition, the post-menopausal phase is accompanied by a progressive proin-flammatory status, which is evidenced by increased systemic IL-1, IL-6, and TNF-α [22], which are potentially important in the pathogenesis of intervertebral disk degeneration, increasing production of matrix degradation enzymes and inhibiting matrix synthesis [23, 24]. Therefore, in the present study, elevated levels of MMP-1 and MMP-13, and therefore activated catabolism of ECM in OVX rat disks, may be due to a deficiency of estrogen. Moreover, the impairments of microstructure and biomechanical properties are also key changes of osteoporotic bone.

Our previous study described the beneficial effects of antiresorptive drugs on disk degeneration in ovariectomized rats; however, alendronate treatment was initiated the day after ovariectomy was performed [8]. In the present study, CT intervention was initiated 12 weeks after ovariectomy was performed, when the osteopenia already existed in the ovariectomized rats. Recent lines of evidence suggest that CT acts on both osteoclasts and chondrocytes. Though the expression is

reduced as rodents age, the CT-receptor (CTR) was identified in bone-matrix-embedded osteocytes [25, 26]. Moreover, articular cartilage chondrocytes from osteoarthritis (OA) patients do indeed express CTR, which makes articular cartilage a pharmacological target for salmon CT [27]. CT treatment increases proteoglycan and collagen synthesis in human osteoarthritic cartilage in vitro [28]. Traumatic OA, augmented by ovariectomy, was reduced by oral salmon CT treatment [29]. The protective effects of CT on IL-1-stimulated chondrocytes in vitro and surgically induced osteoarthritic cartilage in vivo were recently evidenced [7]. The present study may provide a new insight into the potential benefits of CT on joint degenerative disease. CT treatment not only exerted a bone mass preservation effect but also partially maintained disk integrity. ECM metabolism plays a key role in the integrity and function of the intervertebral disk. For further insight into the mechanism of action of CT on disk ECM metabolism, we explored whether MMP-1, MMP-13, and collagen II participate in this process. Breakdown of collagen II in the end plate and annulus fibrosis is a key event in the progression of disk degeneration [30]. OVX+CT animals showed higher expression of collagen II when compared with the OVX+V group. Thus, CT may contribute to ECM integrity. MMPs, including MMP-1 and MMP-13, are thought to be important catabolic enzymes responsible for ECM turnover, such as degrading collagen II [31, 32]. The inhibition of MMP-13 is considered to have a protective effect in the maintenance of intervertebral disk integrity [8]. In line with these assumptions, we have shown that CT treatment decreases enhanced expression of MMP-1 and MMP-13 in the degenerated disk, similar to previous results in articular chondrocytes [10]. The present findings suggest that the beneficial effect of CT treatment on degenerated disks might be partly due to promoting synthesis of collagen II and inhibiting MMP-1 and MMP-13 expression, thereby maintaining the integrity of the ECM during the development of disk degeneration in OVX rats. However, further study is needed to confirm the role for this feature of CT in preventing disk degeneration.

It should be acknowledged, however, that a limitation of the present study is that the analyses of collagen II, MMP-1, and MMP-13 expression in the nucleus pulposus were absent in the present study. As the histological findings suggest, cell type in the nucleus pulposus changed as disk degeneration developed, whereby notochordal cells were replaced by chondrocyte-like cells. These different cell types would likely impact the significance of the data and increase the difficulty of performing cellular detection of collagen II, MMP-1, and MMP-13 expression in the nucleus pulposus. Moreover, though all three groups were treated alike, storing L3 vertebrae in ethanol before biomechanical test is still another weakness of the present study, which may negatively affect biomechanical properties by dehydrating the tissue. Moreover, for the semiquantitative disk degeneration assessment scoring

system, including tissue from rats young enough to have no disk degeneration, would have assured the ability of the method to identify disease-free intervertebral disks.

Taken together, the present study provides the first evidence that preservation of bone mass at the lumbar vertebrae in OVX rats following CT treatment is associated with suppression of intervertebral disk degeneration. The underlying mechanism for this beneficial effect of CT on the degenerated disk might be partially from the modulation of extracellular matrix metabolism and improvement of microstructure parameters and biomechanical properties at the lumbar vertebrae, which need to be confirmed by further study.

References

1. Andersson GB (1999) Epidemiological features of chronic low-back pain. Lancet 354:581–585

2. Boos N, Weissbach S, Rohrbach H, Weiler C, Spratt KF, Nerlich AG (2002) Classification of age-related changes in lumbar intervertebral discs: 2002 Volvo award in basic science. Spine 27:2631–2644

3. Hadjipavlou AG, Tzermiadianos MN, Bogduk N, Zindrick MR (2008) The pathophysiology of disc degeneration: a critical review. J Bone Joint Surg (Br) 90:1261–1270

4. Nanjo Y, Morio Y, Nagashima H, Hagino H, Teshima R (2003) Correlation between bone mineral density and intervertebral disk degeneration in pre- and postmenopausal women. J Bone Miner Metab 21:22–27

5. Fabreguet I, Fechtenbaum J, Briot K, Paternotte S, Roux C (2013) Lumbar disc degeneration in osteoporotic men: prevalence and assessment of the relation with presence of vertebral fracture. J Rheumatol 40:1183–1190

6. Wang YX, Griffith JF (2010) Effect of menopause on lumbar disc degeneration: potential etiology. Radiology 257:318–320

7. Wang T, Zhang L, Huang C, Cheng AG, Dang GT (2004) Relationship between osteopenia and lumbar intervertebral disc degeneration in ovariectomized rats. Calcif Tissue Int 75:205–213

8. Luo Y, Zhang L, Wang WY, Hu QF, Song HP, Su YL, Zhang YZ (2013) Alendronate retards the progression of lumbar intervertebral disc degeneration in ovariectomized rats. Bone 55:439–448

9. Sexton PM, Findlay DM, Martin TJ (1999) Calcitonin. Curr Med Chem 6:1067–1093

10. Sondergaard BC, Wulf H, Henriksen K, Schaller S, Oestergaard S, Qvist P, Tankó LB, Bagger YZ, Christiansen C, Karsdal MA (2006) Calcitonin directly attenuates collagen type II degradation by inhibition of matrix metalloproteinase expression and activity in articular chondrocytes. Osteoarthritis Cartilage 14:759–768

11. Cheng T, Zhang L, Fu X, Wang W, Xu H, Song H, Zhang Y (2013) The potential protective effects of calcitonin involved in coordinating chondrocyte response, extracellular matrix, and subchondral

trabecular bone in experimental osteoarthritis. Connect Tissue Res 54:139–146

12. Shen Y, Li M, Wronski TJ (1997) Calcitonin provides complete protection against cancellous bone loss in the femoral neck of OVX rats. Calcif Tissue Int 60:457–461

13. Mosekilde L, Danielsen CC, Knudsen UB (1993) The effect of aging and ovariectomy on the vertebral bone mass and biomechanical properties of mature rats. Bone 14:1–6

14. Allon AA, Aurouer N, Yoo BB, Liebenberg EC, Buser Z, Lotz JC (2010) Structured coculture of stem cells and disc cells prevent disc degeneration in a rat model. Spine J 10:1089–1097

15. Yuan M, Qiu M, Cui J, Zhang X, Zhang P (2014) Protective effects of pioglitazone against immunoglobulin deposition on heart of streptozotocin-induced diabetic rats. J Endocrinol Invest 37:375–384

16. de Schepper EI, Damen J, van Meurs JB, Ginai AZ, Popham M, Hofman A, Koes BW, Bierma-Zeinstra SM (2010) The association between lumbar disc degeneration and low back pain: the influence of age, gender, and individual radiographic features. Spine (Phila Pa 1976) 35:531–536

17. Wang YX, Griffith JF, Ma HT, Kwok AW, Leung JC, Yeung DK, Ahuja AT, Leung PC (2011) Relationship between gender, bone mineral density, and disc degeneration in the lumbar spine: a study in elderly subjects using an eight-level MRI-based disc degeneration grading system. Osteoporos Int 22:91–96

18. Wang YX, Kwok AW, Griffith JF, Leung JC, Ma HT, Ahuja AT, Leung PC (2011) Relationship between hip bone mineral density and lumbar disc degeneration: a study in elderly subjects using an eight-level MRI-based disc degeneration grading system. J Magn Reson Imaging 33:916–920

19. Baron YM, Brincat MP, Galea R, Calleja N (2005) Intervertebral disc height in treated and untreated overweight post-menopausal women. Hum Reprod 20:3566–3570

20. Wang Y, Boyd SK, Battié MC, Yasui Y, Videman T (2011) Is greater lumbar vertebral BMD associated with more disk degeneration? A study using μCT and discography. J Bone Miner Res 26:2785–2791

21. Mattei TA (2013) Osteoporosis delays intervertebral disc degeneration by increasing intradiscal diffusive transport of nutrients through both mechanical and vascular pathophysiological pathways. Med Hypotheses 80:582–586

22. Zheng SX, Vrindts Y, Lopez M, De Groote D, Zngerle PF, Collette J, Franchimont N, Geenen V, Albert A, Reginster JY (1997) Increase in cytokine production (IL-1b, IL-6, TNF-a but not IFN-g, GM-CSF or LIF) by stimulated whole blood cells in postmenopausal osteoporosis. Maturitas 26:63–71

23. Phillips KL, Jordan-Mahy N, Nicklin MJ, Le Maitre CL (2013) Interleukin -1 receptor antagonist deficient mice provide insights into pathogenesis of human intervertebral disc degeneration. Ann Rheum Dis 72:1860–1867

24. Séguin CA, Pilliar RM, Roughley PJ, Kandel RA (2005) Tumor necrosis factor-alpha modulates matrix production and catabolism in nucleus pulposus tissue. Spine (Phila Pa 1976) 30:1940–1948

25. Gooi JH, Chia LY, Walsh NC, Karsdal MA, Quinn JM, Martin TJ, Sims NA (2014) Decline in calcitonin receptor expression in osteocytes with age. J Endocrinol 221:181–191

26. Gooi JH, Pompolo S, Karsdal MA, Kulkarni NH, Kalajzic I, McAhren SH, Han B, Onyia JE, Ho PW, Gillespie MT, Walsh NC, Chia LY, Quinn JM, Martin TJ, Sims NA (2010) Calcitonin impairs the anabolic effect of PTH in young rats and stimulates expression of sclerostin by osteocytes. Bone 46:1486–1497

27. Segovia-Silvestre T, Bonnefond C, Sondergaard BC, Christensen T, Karsdal MA, Bay-Jensen AC (2011) Identification of the calcitonin receptor in osteoarthritic chondrocytes. BMC Res Notes 4:407

28. Sondergaard BC, Madsen SH, Segovia-Silvestre T, Paulsen SJ, Christiansen T, Pedersen C, Bay-Jensen AC, Karsdal MA (2010) Investigation of the direct effects of salmon calcitonin on human osteoarthritic chondrocytes. BMC Musculoskelet Disord 11:62

29. Nielsen RH, Bay-Jensen AC, Byrjalsen I, Karsdal MA (2011) Oral salmon calcitonin reduces cartilage and bone pathology in an osteoarthritis rat model with increased subchondral bone turnover. Osteoarthritis Cartilage 19:466–473

30. Le Maitre CL, Pockert A, Buttle DJ, Freemont AJ, Hoyland JA (2007) Matrix synthesis and degradation in human intervertebral disc degeneration. Biochem Soc Trans 35:652–655

31. Le Maitre CL, Freemont AJ, Hoyland JA (2004) Localization of degradative enzymes and their inhibitors in the degenerate human intervertebral disc. J Pathol 204:47–54

32. Pelletier JP, Kapoor M, Fahmi H, Lajeunesse D, Blesius A, Maillet J, Martel-Pelletier J (2013) Strontium ranelate reduces the progression of experimental dog osteoarthritis by inhibiting the expression of key proteases in cartilage and of IL-1β in the synovium. Ann Rheum Dis 72:250–257